Micellar Dissolution and Diffusion Effects on Adsorption Dynamics of Surfactants

Ying-Chih Liao, Osman A. Basaran, and Elias I. Franses
School of Chemical Engineering, Purdue University, West Lafayette, IN 47907

A one-dimensional (1-D) model for the diffusion-controlled dynamic adsorption and surface tension in micellar solutions of nonionic surfactants is developed and tested with experimental data. The micellar dissolution rate for monodisperse micelles is described as being proportional to the micellar concentration and to the concentration difference between the critical micelle concentration (cmc) and the local monomer concentration with a micellar dissolution rate constant k. The Langmuir or Frumkin adsorption isotherms are used in a diffusion-controlled adsorption model with micellar dissolution. The hydrodynamic effects due to interface generation in the experiments are simplified as resulting in a stagnant layer with an adjustable finite length l. The model is solved rigorously by the finite-element method with a stretched grid and adaptive time step sizes. From simulations, the micellar dissolution rate is found to be much more important for dynamic adsorption than the micellar diffusion rate. Moreover, the size distribution of micelles is found to be insignificant for dynamic adsorption when a narrow distribution is considered. New equilibrium and dynamic surface-tension data for a planar interface in a Langmuir trough has been obtained for two nonionic surfactants, straight-chain alkyl ethylene oxides, $C_{14}E_6$ and $C_{16}E_6$, at concentrations below and above their cmc's. The pre-cmc data are used to obtain the respective Langmuir isotherm parameters $\Gamma_{m,L}$ and K_L and the effective diffusion length $l \approx 0.3$ mm. With values of $\Gamma_{m,L}$, K_L, and l determined from pre-cmc data, the post-cmc data are fitted fairly well with the micellar dissolution time constant $\tau_K \equiv 1/kC^*$ (C^* is the cmc), which is 1.2 ms for $C_{14}E_6$ and 4.5 ms for $C_{16}E_6$.

Introduction

The dynamic adsorption of a single nonionic surfactant solution below its critical micelle concentration (cmc) in a stagnant medium has been studied for several decades and is well established (Ward and Tordai, 1946; Lin et al., 1990; Chang and Franses, 1995; Ferri and Stebe, 2000). For many applications, however, surfactants are used above or well above their cmc (Rosen, 1978). Even though the equilibrium surface tension of surfactant solutions above their cmc is nearly constant, the tension and adsorption dynamics become faster with higher micelle concentration. Applications, such as foaming, coating, wetting, and emulsification, involve fast adsorption in micellar solutions. Hence, it is important to understand the role of micelles on adsorption dynamics.

The presence of micelles in the bulk solution can affect the adsorption dynamics strongly, because micelles can replenish the loss of surfactant monomers due to their diffusion and adsorption, and hence increase the net rate of adsorption (Filippov and Filippova, 1997; Noskov, 2002). The dynamic adsorption process is shown in Figure 1. Initially, the micelles are in dynamic equilibrium with the monomers in the solution. Adsorption of monomers at the interface causes a concentration gradient, which makes the monomers to diffuse to the interface and reduces their concentration in the bulk. Then, the micelles are no longer at equilibrium with the monomers and start dissolving, or releasing monomers. To account for the effects of micelles, one needs to model the mechanism of micellar dissolution kinetics along with micellar diffusion.

Among several proposed micellar kinetic models, the stepwise aggregation model is the most plausible and the most complex (Dukhin et al., 1995). In this model, one assumes that the micelles aggregate or dissociate in a series of steps.

Correspondence concerning this article should be addressed to E. I. Franses.

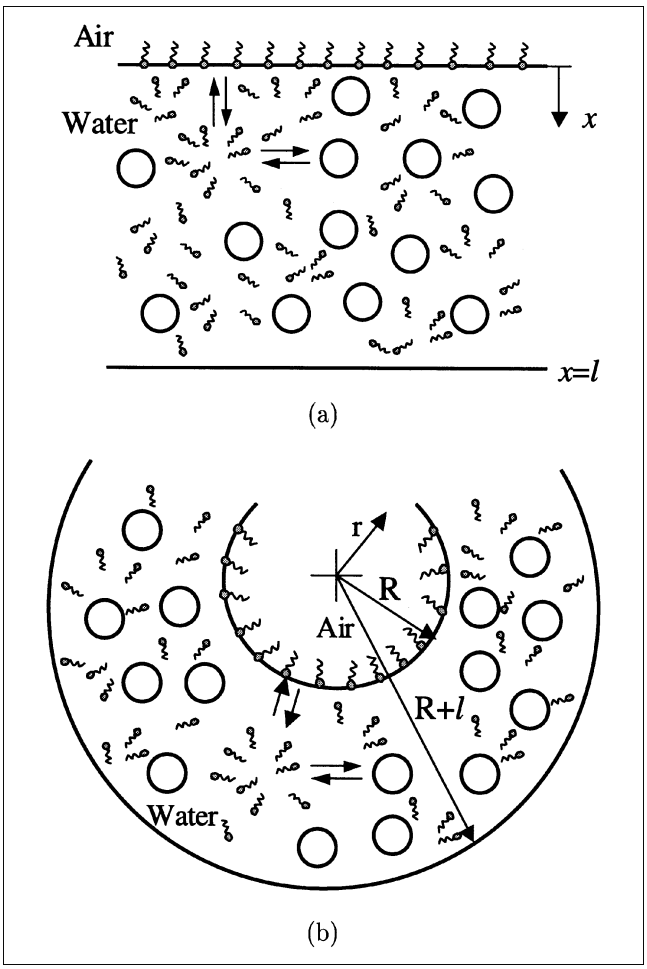

Figure 1. Micellar dissolution and dynamic adsorption (a) at a planar interface and (b) around an air bubble (not to scale).

In each step, a monomer is added to or released from a micelle. Therefore, one needs two rate constants, for aggregation and dissociation, respectively, to describe each step. Consequently, for a distribution of micelles, many rate constants are needed to describe the whole process of micellar aggregation and dissociation. These rate constants are related to the stepwise micellar formation equilibrium, which yields the micelle aggregation number distribution and the average aggregation number $\overline{N}$ (Nagarajan and Ruckenstein, 2000). With several further assumptions and a population balance approach, Aniansson and Wall (1974) characterized the stepwise dissociation for perturbation around the equilibrium distribution with two relaxation time scales, τ_1 and τ_2, but with no dependence of these time scales on spatial coordinates. When the micellar size distribution undergoes small deviations from the equilibrium micellar distribution, for example, when the average aggregation number changes from $\overline{N}$ to $\overline{N}-1$, this "fast process" is complete in times of the order of τ_1, which ranges from μs to ms (Pillai and Shah, 1995). For large deviations from the equilibrium, or for micelles dissociating totally into monomers, the process is slower, and is of the order of τ_2, which ranges from seconds to over 100 s (Patist et al., 2001). Dushkin et al. (1991) have determined the effects of slow and fast micellar dissociation on the adsorption dynamics, and developed a model for the dynamic adsorption on the surface of a thin film (Dushkin, 1998). This model is then solved approximately with analytical linearization methods, and is limited to small deviations from equilibrium.

In another model, one assumes that monodisperse micelles, with aggregation number, N, totally dissolve to produce N monomers (Lucassen, 1976; Miller, 1981). For this mechanism, described as an Nth-order reaction, the net dissolution rate from micelles is assumed to be

$$J_1 = N\left(k_d C_N - k_f C_1^N\right) \tag{1}$$

where C_1 and C_N are the concentrations of monomers and micelles, and k_f and k_d are rate constants for micellar formation and dissolution. This model is thermodynamically consistent, that is, at equilibrium ($J_1 = 0$), the ratio C_1^N/C_N is constant, as expected from the equilibrium constant condition for monodisperse micelles. Nevertheless, since most intrinsic reaction orders cannot be higher than three or four (Hill, 1977), this model seems implausible for describing micellar kinetics.

In another model suggested by Fainerman et al. (1984), who consider the relaxation of micellar dissociation with slow and fast processes, the net rate of micellar dissolution is

$$J_1 = k_1 C_N (C^* - C_1)\left[1 - \xi \exp(-tk_2)\right]\left[q + \frac{C_N}{C^*}\right] \tag{2}$$

where k_1 and k_2 are dissolution rate constants for fast and slow processes, C^* is the cmc, ξ and q are parameters, and t is time. This model has been adopted by Zhmud et al. (2000), who reported some sample calculations, but did not determine specific values for the parameters.

At high micellar concentrations, at which the fast dissolution process can be a rate-determining step, Fainerman (1981) suggested the following simple equation

$$J_1 = kC_N (C^* - C_1) \tag{3}$$

where k is the dissolution rate constant. For micelles in an ideal solution, the equilibrium monomer concentration around each micelle is expected to be equal to the cmc or C^* (Evans and Wennerström, 1999). The dissolution of micelles would be similar to the dissolution process of a crystallite or droplet at a solid/liquid or liquid/liquid interface (Figure 2), and the net dissolution rate is proportional to the driving force $C^* - C_1$. Thus, the constant k in Eq. 3 is analogous to an overall mass-transfer coefficient (Figure 2). Moreover, the net dissolution rate J_1 is expected to increase proportionally to the exposed micellar interfacial area, which is proportional to C_N for a fixed value of N.

It remains unclear that complex models are needed to adequately describe the essence of experimental data of dynamic adsorption from micellar solutions. For this reason, in this article, we use and test the simple Eq. 3 coupled with the equations for diffusion and adsorption/desorption. We solve

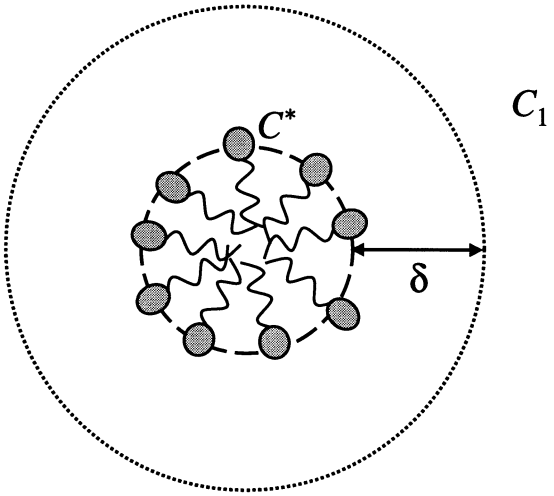

Figure 2. Micellar dissolution near a micelle: at the micelle/solution interface, the monomer concentration is taken to be equal to the cmc C^*.

In the bulk solution, at a distance δ, which depends on the micelle concentration, the monomer concentration under nonequilibrium condition is C_1. The driving force for mass transfer is $C^* - C_1$. The net mass-transfer rate is $k^*(C^* - C_1)A$, where A is the micelle area and k^* is a mass-transfer coefficient. For monodisperse, fixed-size micelles with aggregation number N, A is a constant and $kC_N = k^*A$.

the resulting model rigorously with the finite-element method for the first time for this problem, without any approximations or linearizations. The model applies to nonionic surfactants with diffusion, but no explicit consideration for convection. It can be generalized to include hydrodynamic effects explicitly, as was done for the first time by Schunk (1989). Here, convection is considered implicitly, in as much as it affects the effective diffusion length of a layer near the interface. We examine the effects of micellar dissolution and diffusion rates in the overall adsorption rate, and identify key dimensionless groups, which can describe when these effects are important. The model is shown to be adequate for describing new experimental data for two typical nonionic surfactants. The micelle dissolution rates are determined to depend on the surfactant hydrophobicity.

Mathematical Model and Solution Method

Model for planar coordinates

For dynamic adsorption of a nonionic surfactant above its cmc, monomer molecules are transported through a diffusion layer of length l, and adsorb onto the air/water (or other fluid) interface (Figure 1a). After the monomers adsorb, a concentration gradient develops. Simultaneously, the micelle/monomer equilibrium is disturbed by monomer diffusion, and micelles release monomers to the bulk solution. The net dissolution of micelles replenishes the loss of bulk monomers, and increases the net rate of dynamic adsorption over what would be in the absence of micelles. For a completely stagnant medium in a long liquid column, the effective diffusion length, l, would be practically infinite. Because of mixing, however, or convection associated with interface formation or with temperature gradients, one should consider the flow explicitly, which makes the problem quite complex. Alternately, one can use diffusion only within a finite effective diffusion length, l (Chang and Franses, 1992, 1995). The latter approach is used in this article. The transport of surfactant monomers and monodisperse micelles of aggregation number N in the bulk solution within the length l is described by the diffusion equations in planar coordinates for $0 < x < l$ and $t > 0$

$$\frac{\partial C_1}{\partial t} = D_1 \frac{\partial^2 C_1}{\partial x^2} + J_1, \tag{4}$$

$$\frac{\partial C_N}{\partial t} = D_N \frac{\partial^2 C_N}{\partial x^2} - \frac{J_1}{N} \tag{5}$$

where x is the distance measured from the interface and D_1 and D_N are the diffusivities of monomers and micelles, respectively; the dissolution rate of micelles J_1 is defined in Eq. 3. For spherical micelles, the micelle diameter is proportional to the cube root of the aggregation number, N. The Stokes-Einstein equation (Cussler, 1984) predicts that the diffusivity of micelles is inversely proportional to the diameter, or $D_N/D_1 = N^{-1/3}$. For nonspherical molecules or micelles, a small correction factor may be needed.

The initial concentrations of monomers and micelles for $0 \le x \le l$ are

$$C_1(x,0) = C^*, \tag{6}$$

and

$$C_N(x,0) = C_{N0} = \frac{C_T - C^*}{N} \tag{7}$$

where C_T is the total concentration. For a newly created clean surface, the surface density is essentially zero at the beginning of the adsorption process

$$\Gamma(0) = 0 \tag{8}$$

although in certain experiments the first measurement is obtained when

$$\Gamma(0) = \Gamma_0 \neq 0 \tag{9}$$

The boundary conditions at $x = 0$ for $t > 0$ are

$$\frac{d\Gamma}{dt} = D_1 \left.\frac{\partial C_1}{\partial x}\right|_{x=0} \tag{10}$$

for monomers, and

$$D_N \left.\frac{\partial C_N}{\partial x}\right|_{x=0} = 0 \tag{11}$$

for micelles, which are assumed not to adsorb at the interface.

Beyond the diffusion layer, the concentrations of monomers and micelles are constant. At $x = l$, the boundary conditions for $t > 0$ are

$$C_1(l,t) = C^*, \tag{12}$$

$$C_N(l,t) = C_{N0} \tag{13}$$

If l is equal to the total thickness of the liquid layer in a container, one may need to use the no-flux boundary condition at $x = l$.

Along with Eqs. 4–13, an additional relation exists between $\Gamma(t)$ and $C_1(0, t)$. Such a relation depends on the "mechanism" of adsorption, by which is meant whether the adsorption is diffusion-controlled, or kinetic-controlled, or "mixed kinetics," that is, affected by both diffusion and adsorption/desorption rate (Chang and Franses, 1995). In this article, we consider the more common first case, where the surface density $\Gamma(t)$ and the subsurface layer concentration $C_1(0, t)$ are in local equilibrium, or where the adsorption/desorption process is much faster than diffusion. Then, $\Gamma(t)$ vs. $C_1(0,t)$ is the dynamic adsorption isotherm, which is normally taken to have the same functional form as the equilibrium adsorption isotherm. A widely used equilibrium isotherm is the Frumkin isotherm

$$\Gamma_e = \Gamma_{m,F} \frac{K_F C_0}{e^{AX_e} + K_F C_0} \tag{14}$$

where Γ_e is the equilibrium surface density, $\Gamma_{m,F}$ is the maximum surface density, K_F is the adsorption equilibrium constant, C_0 is the equilibrium concentration of monomers, A is the binary interaction parameter, and $X_e \equiv \Gamma_e/\Gamma_{m,F}$ is the equilibrium surface coverage. The dynamic Frumkin isotherm is

$$\Gamma(t) = \Gamma_{m,F} \frac{K_F C_1(0,t)}{e^{AX(t)} + K_F C_1(0, t)} \tag{15}$$

where $X(t) \equiv \Gamma(t)/\Gamma_{m,F}$ is the dynamic surface coverage. The dynamic surface tension $\gamma(t)$ is obtained from the dynamic Frumkin equation of state

$$\gamma(t) - \gamma_0 = \Gamma_{m,F} RT \left\{ \ln[1 - X(t)] - \frac{AX(t)^2}{2} \right\} \tag{16}$$

where γ_0 is the surface tension of the pure liquid. For $A = 0$, the Frumkin isotherm reduces to the well-known Langmuir isotherm. Then, the parameters $\Gamma_{m,F}$ and K_F are replaced by $\Gamma_{m,L}$ and K_L, which have the same meaning.

Model for spherical coordinates

This model is needed when one uses a spherical bubble method (Franses et al., 1996), in which diffusion to the interface from the liquid phase is inward (toward the bubble center), or a drop method, in which diffusion to the interface is outward. Similarly to the model in planar coordinates, for a spherical bubble with a radius, R, and an effective diffusion length, l (Figure 1b), the transport of monomers and micelles is described by the diffusion equations in spherical coordinates for $R < r < R + l$ and $t > 0$

$$\frac{\partial C_1}{\partial t} = \frac{D_1}{r^2} \frac{\partial}{\partial r} \left(r^2 \frac{\partial C_1}{\partial r} \right) + J_1, \tag{17}$$

$$\frac{\partial C_N}{\partial t} = \frac{D_N}{r^2} \frac{\partial}{\partial r} \left(r^2 \frac{\partial C_N}{\partial r} \right) - \frac{J_1}{N} \tag{18}$$

The initial conditions are

$$C_1(r,0) = C^*, \tag{19}$$

$$C_N(r,0) = C_{N0} \tag{20}$$

and

$$\Gamma(0) = 0 \qquad \text{or} \qquad \Gamma(0) = \Gamma_0 \neq 0 \tag{21}$$

The boundary conditions at $r = R$ and $r = R + l$ for $t > 0$ are

$$\frac{d\Gamma}{dt} = D_1 \left. \frac{\partial C_1}{\partial r} \right|_{r=R}, \tag{22}$$

$$D_N \left. \frac{\partial C_N}{\partial r} \right|_{r=R} = 0, \tag{23}$$

$$C_1(R + l,t) = C^*, \tag{24}$$

$$C_N(R + l,t) = C_{N0} \tag{25}$$

The dynamic Frumkin isotherm and its equation of state are the same as in Eqs. 15 and 16, except that the term $C_1(0,t)$ in planar coordinates is replaced by $C_1(R,t)$. This model reduces to the planar model when $R \to \infty$ or $R \gg l$.

Dimensionless equations and groups for spherical coordinates

For the convenience of further mathematical treatment, and for helping to identify the key dimensionless groups, the concentration, surface density, distance, and time are nondimensionalized as

$$u_1 \equiv \frac{C_1}{C^*}, \tag{26}$$

$$u_N \equiv \frac{C_N}{C_{N0}}, \tag{27}$$

$$\theta \equiv \frac{\Gamma}{\Gamma_e}, \tag{28}$$

$$\rho \equiv \frac{r - R}{l} \tag{29}$$

$$\tau \equiv \frac{t}{\tau_D} \tag{30}$$

Here the characteristic time scale is defined as

$$\tau_D \equiv L^2/D_1 \tag{31}$$

where the characteristic length L is the length of depletion, or the thickness of the solution at the cmc containing the same amount of surfactant as in the equilibrium surface layer

$$L \equiv \Gamma_e / C^* \tag{32}$$

The time for a new air/water surface with nonionic surfactant solutions below or at the cmc to reach equilibrium is usually between 1 and 10 τ_D (Ferri and Stebe, 2000). For several nonionic surfactants, if one uses the Langmuir isotherm, which is a special case of the Frumkin isotherm with $A = 0$, one can find $\Gamma_{m,L}$ and K_L, from which one can calculate L and τ_D (Table 1). Typical values of τ_D for nonionic surfactants, range from 30 ms to 4.5×10^5 s. These values indicate that the diffusion can be slower than the micellar dissolution, which can then affect the net adsorption rate.

The dimensionless diffusion layer thickness is defined as

$$N_l \equiv \frac{l}{L} = \frac{lC^*}{\Gamma_e} \tag{33}$$

The smaller the value of N_l, the higher the adsorption rate is expected to be for diffusion-controlled adsorption. The dimensionless bubble size is

$$N_R \equiv \frac{R}{l} \tag{34}$$

For $N_R \gg 1$, the interface is effectively planar.

The dimensionless counterparts of Eqs. 17–25 are

$$N_l^2 \frac{\partial u_1}{\partial \tau} = \frac{1}{(\rho + N_R)^2} \frac{\partial}{\partial \rho}\left[(\rho + N_R)^2 \frac{\partial u_1}{\partial \rho}\right] + \bar{J}_1, \tag{35}$$

$$N_l^2 \frac{\partial u_N}{\partial \tau} = \frac{S}{(\rho + N_R)^2} \frac{\partial}{\partial \rho}\left[(\rho + N_R)^2 \frac{\partial u_N}{\partial \rho}\right] - \frac{\bar{J}_1}{T-1}, \tag{36}$$

$$\bar{J}_1 = N_D N_l^2 \frac{T-1}{N} u_N (1 - u_1), \tag{37}$$

$$u_1(\rho, 0) = 1, \tag{38}$$

$$u_N(\rho, 0) = 1, \tag{39}$$

$$\theta(0) = 0, \tag{40}$$

$$N_l \frac{d\theta}{d\tau} = \left.\frac{\partial u_1}{\partial \rho}\right|_{\rho = 0}, \tag{41}$$

$$\left.\frac{\partial u_N}{\partial \rho}\right|_{\rho = 0} = 0, \tag{42}$$

$$u_1(1, \tau) = 1, \tag{43}$$

$$u_N(1, \tau) = 1 \tag{44}$$

where $S \equiv D_N / D_1$ is the diffusivity ratio, $T \equiv C_T / C^*$ is the dimensionless total concentration, and the dimensionless dissolution rate constant N_D is given by

$$N_D \equiv kC^* \tau_D = \frac{kC^* L^2}{D_1} \tag{45}$$

The parameter N_D is the ratio of the diffusion time scale τ_D and the micelle dissolution time scale $\tau_k \equiv 1/kC^*$. A large value of $N_D \equiv \tau_D / \tau_k$ means that the micellar dissolution is much faster than the monomer diffusion, and $N_D \ll 1$ means that micellar dissolution is unimportant. We conjecture that the dissolution time scale τ_k is related to the fast micellar "relaxation" time scale τ_1, which is of the order from 10^{-6} to 10^{-3} s. Given the range of the values of τ_k and τ_D, one finds that N_D can vary from 10^1 to 10^{11} (see the Results and Discussion section).

The dimensionless dynamic Frumkin isotherm is

$$\theta(\tau) = \frac{N_c u_s}{X_e\left(e^{AX_e\theta} + N_c u_s\right)} \tag{46}$$

where $u_s(\tau) \equiv u(0, \tau)$ is the dimensionless subsurface layer concentration, and $N_c \equiv K_F C^*$ is the dimensionless concentration. The dimensionless surface pressure Π is

$$\Pi \equiv \frac{\gamma_0 - \gamma(\tau)}{\gamma_0 - \gamma_e} = \frac{\ln(1 - X_e\theta) - \frac{A}{2} X_e^2 \theta^2}{\ln(1 - X_e) - \frac{A}{2} X_e^2} \tag{47}$$

where γ_e is the equilibrium surface tension. Equations 35–46 are solved numerically with the finite-element method described in the next section.

Finite-element analysis

Equations 35 to 44 are solved rigorously for the first time using a method of lines that incorporates the Galerkin finite element (FE) method (Strang and Fix, 1973) for spatial discretization and an adaptive finite difference method for time integration (Liao et al., 2003; Zhang et al., 1996). The spatial domain $0 \le \rho \le 1$ is divided into N_E elements. The monomer and micelle concentration profiles are then expanded in terms of a series of quadratic basis function $\phi^j(\rho)$

$$u_1(\rho, \tau) = \sum_{j=1}^{N_x} u_{1_j}(\tau) \phi^j(\rho) \tag{48}$$

$$u_N(\rho, \tau) = \sum_{j=1}^{N_x} u_{N_j}(\tau) \phi^j(\rho), \tag{49}$$

where u_{1_j} and u_{N_j} are unknown coefficients to be determined and $N_x = 2N_E + 1$ is the total number of nodes. The Galerkin weighted residuals for Eqs. 35 and 36 are constructed by weighting the differential equations with the quadratic basis function $\phi^i(\rho)$, integrating the resulting expressions over the spatial domain, and rearranging the inte-

grals by integration by parts

$$R_1^i = \int_0^1 \left(N_l^2 \frac{\partial u_1}{\partial \tau}\phi^i + \frac{\partial u_1}{\partial \rho}\frac{d\phi^i}{d\rho} - \bar{J}_1\phi^i \right) \times (\rho + N_R)^2\, d\rho - \phi^i(\rho + N_R)^2 \frac{\partial u_1}{\partial \rho}\bigg|_{\rho=0}^{\rho=1} = 0,$$

$$R_N^i = \int_0^1 \left(N_l^2 \frac{\partial u_N}{\partial \tau}\phi^i + S\frac{\partial u_N}{\partial \rho}\frac{d\phi^i}{d\rho} - \frac{\bar{J}_1}{T-1}\phi^i \right)(\rho + N_R)^2\, d\rho - \phi^i S(\rho + N_R)^2 \frac{\partial u_N}{\partial \rho}\bigg|_{\rho=0}^{\rho=1} = 0, \quad i = 1, 2, \ldots, N_x. \quad (50)$$

The weighted residual equation set, Eq. 50, can be simplified by means of the boundary conditions Eqs. 41–44

$$R_1^i = \int_0^1 \left(N_l^2 \frac{\partial u_1}{\partial \tau}\phi^i + \frac{\partial u_1}{\partial \rho}\frac{d\phi^i}{d\rho} - \bar{J}_1\phi^i \right) \times (\rho + N_R)^2\, d\rho + \delta_{i1} N_l N_R^2 \frac{d\theta}{d\tau} = 0,$$

$$R_N^i = \int_0^1 \left(N_l^2 \frac{\partial u_N}{\partial \tau}\phi^i + S\frac{\partial u_N}{\partial \rho}\frac{d\phi^i}{d\rho} - \frac{\bar{J}_1}{T-1}\phi^i \right) \times (\rho + N_R)^2 d\rho = 0, \qquad i = 1, 2, \ldots, N_x - 1,$$

$$R_1^{N_x} = 1,$$

$$R_N^{N_x} = 1 \quad (51)$$

A stretched-grid-generation method is used to minimize the number of nodes while maintaining numerical accuracy (Knupp and Steinberg, 1993). This method allows more nodes to be used near the interface where the concentration gradients are large compared to the rest of the domain. The size of each element is determined by an exponential function, and the middle node of each element is located halfway between the two end nodes, namely

$$\sigma_i = \frac{i}{N_E}, \qquad i = 1, 2, \ldots, N_E,$$

$$\rho_1 = 0, \qquad \rho_{2i+1} = \frac{e^{\lambda\sigma_i} - 1}{e^{\lambda} - 1},$$

$$\rho_{2i} = \frac{\rho_{2i-1} + \rho_{2i+1}}{2} \quad (52)$$

The positive parameter λ is determined by placing one element across the penetration depth of the concentration profile $\rho_d = \sqrt{\tau}/N_l$ during the first time step $\tau^{(1)}$

$$\frac{e^{\lambda/N_E} - 1}{e^{\lambda} - 1} = \frac{\sqrt{\tau^{(1)}}}{N_l}. \quad (53)$$

The time derivatives of u_{1j}, u_{Nj}, and θ are formulated with either the backward-difference method or the trapezoidal rule over a time interval $\Delta\tau^{(p)} = \tau^{(p)} - \tau^{(p-1)}$, $p = 1, 2, \ldots$. Four backward-difference time steps with fixed time-step size $\Delta\tau = 10^{-4}$ are used initially to provide the necessary smoothing (Luskin and Rannacher, 1982). In the subsequent steps, a second-order Adams-Bashforth predictor is used with the trapezoidal rule to evaluate the relative time truncation errors and the time-step sizes adaptively. Finally, the system comprising Eqs. 51 and 46 of $2N_x + 1$ nonlinear algebraic equations is solved by Newton's method.

Materials and Methods

Materials

Nonionic alkyl ethylene oxides surfactants (polyethylene glycol monoalkyl ether), $C_{14}E_6$ and $C_{16}E_6$, of purity 99+%, were purchased from Fluka (Milwaukee, WI). These two surfactants were chosen because they have large τ_D (>1,000 s; see Table 1) so that the measurements can detect the full range of the dynamic adsorption process. The water used for all samples was first distilled and then passed through a Millipore four-stage cartridge system, resulting in a water resistivity of 18 MΩ·cm at the exit port. Fresh surfactant solu-

Table 1. Data and Properties of Nonionic Surfactants

		$C_{10}E_6$	$C_{12}E_6$	$C_{12}E_5$	$C_{14}E_6$	$C_{16}E_6$	Triton X100
MW	dalton	423	451	407	479	507	624
$\Gamma_{m,L}$	μmol/m^2	2.4**	2.7**	7.5*	3.7*	6.0*	2.9†
K_L	m^3/mol	700**	5,000**	220*	14,000*	26,500*	1,500†
cmc (C^*)	mol/m^3	0.9**	0.08**	0.04*	0.006*	0.0005*	0.23†
N_C^{*}††	—	630	400	8.8	84	13.25	345
$D_1\times10^{10}$	m^2/s‡	2.96	2.90	3.00	2.84	2.79	2.60†
τ_D‡‡	s	0.03	4.5	103	1,240	4.5×10^5	0.61
N§	—	NA	200	200	NA	250	NA
$1/kC^*$	ms	NA	NA	NA	1.2	4.5	NA
k	m^3/mol/s	NA	NA	NA	1.39×10^5	4.4×10^5	NA

*Best-fit values; see Figure 3.
**Values from Zhmud et al. (2000).
†Values from Lin et al. (1990).
††Dimensionless concentration at cmc $N_C^* \equiv K_F C^*$.
‡Calculated from Stokes-Einstein equation.
‡‡Characteristic time scale at cmc $\tau_D \equiv \Gamma_e^2/(D_1 C^{*2})$.
§Micelle aggregation numbers predicted by Nagarajan and Ruckenstein (2000).

tions (less than one day old) were used for all the dynamic surface-tension (DST) measurements.

Surface-tension measurements

A KSV Langmuir standard-trough, from KSV Instruments, Finland, with a dipping well and a roughened platinum Wilhelmy plate, was used to obtain DST vs. time data and equilibrium surface tensions (± 0.5 mN/m). The solutions were placed in the dipping well, which has dimensions of $3.7 \times 11.6 \times 9.1$ cm. The temperature was controlled at 24 ± 0.5°C. To clean the surface from possible impurities, and for testing the reproducibility of the DST data, the surface was created by fast wiping the interface with a delrin-taped barrier by hand at least ten times. Then, the surface was further aspirated with a pipette before data collection. This wiping and aspiration process leads to convective flow, which stops after a few seconds. Hence the effective value of l should be initially small and increase with time. Such a time variation of l would have to be evaluated by solving the relevant hydrodynamic equations, which include the effects of actual system geometry. Unfortunately, doing so results in a problem that is both complicated and no longer one-dimensional. Here, for the simplicity of the model, a fixed l value is used in the fitting procedure, and its effectiveness is tested with the data.

Surface-tension data were collected as follows. First, pure water was placed in the dipping well, and the balance connected to the platinum Wilhelmy plate was zeroed. Then, the pure water was replaced with a surfactant solution. The surface was aspirated until the initial surface pressure ($\gamma_0 - \gamma$) was at least no more than 5 mN/m, and the dynamic surface-pressure data were collected afterward. Because of some adsorption while the surface is aspirated, a completely surfactant-free surface ($\Gamma = 0$ and $\Pi = 0$) is hard to obtain at the time of the first measurement ($t \approx 0$). The initial value of the surface density was nonzero and was obtained from the measured value of the first surface-tension measurement, that is, $\Gamma[\gamma(t = 0)]$. The equilibrium surface tensions at different concentrations were defined as the steady-state values of DST, if they remained constant for at least 20 min.

The equilibrium bulk concentrations were unequal to the initial concentration because of adsorption. The equilibrium concentrations were found by subtracting the adsorption loss, $C_0 = C_{initial} - A\Gamma_e/V$, where Γ_e was estimated from the equilibrium isotherm, and A and V are the area and volume of the dipping well. The correction for 10^{-4} mol/m^3 was about 20%. For $C_{initial} < 10^{-4}$ mol/m^3, there is a big correction due to adsorption, and the equilibration time might be several days, making the data unreliable. For these reasons, no data were reported for $C_{initial} < 10^{-4}$ mol/m^3. The limited equilibrium data (Figure 3) did not justify using the three-parameter Frumkin isotherm. Hence, for fitting the data, we used the two-parameter Langmuir isotherm. The best-fitted values (Table 1) were used for the calculation of the adsorption dynamics.

Evaluation of key parameters

The molecular diffusivities of several nonionic surfactants (Table 1) were estimated based on the published diffusivity of Triton X100, $D_{Tr} = 2.6 \times 10^{-10}$ m^2/s (Lin et al., 1990), and the ratio of the molecular weight of these surfactants to that of Triton X100 using the Stokes-Einstein equation

$$\frac{D_{C_mE_n}}{D_{Tr}} = \left[\frac{M.W._{\cdot C_mE_n}}{M.W._{\cdot Tr}}\right]^{-1/3} \tag{54}$$

The aggregation numbers N for $C_{12}E_6$ and $C_{16}E_6$ were found to be around 200 and 250 in the literature (Nagarajan and Ruckenstein, 2000). The value of N for $C_{14}E_6$ was estimated to be between the two values just given. In the following section, we will show that small variation of micelle size N is not practically important, and hence the value of N was set to be 216 for both $C_{14}E_6$ and $C_{16}E_6$ in the simulations. The diffusivity ratio S, following the Stokes-Einstein equation, would be $S \equiv D_N/D_1 = N^{-1/3} = 0.16$.

In the adsorption problem for a nonionic surfactant below its cmc, the parameters $\Gamma_{m,L}$ and K_L are known from the equilibrium isotherm; D_1 is found by Eq. 54. The only adjustable parameter, l, is determined by fitting the DST data for all concentrations below or equal to the cmc. For post-cmc concentrations, we used the same values of $\Gamma_{m,L}$, K_L, D_1, and l as in the sub-cmc cases. The remaining unknown parameter, k, is then determined by fitting the post-cmc DST data at various concentrations. The scheme is simple and self-consistent, and should work to the extent that the adsorption is diffusion-controlled and governed by the Langmuir isotherm.

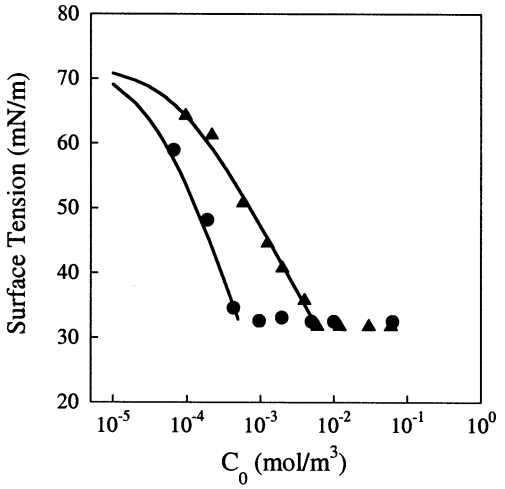

Figure 3. Equilibrium surface tension data for $C_{14}E_6$ (▲) and $C_{16}E_6$ (●).

The data are fitted using the Langmuir-Szyszkowsky isotherm (solid lines), and the best-fit parameters are listed in Table 1. The average standard deviation for the fitted isotherms is ca 1 mN/m.

Results and Discussion

Effects of key dimensionless groups

Several key properties of nonionic surfactants are summarized in Table 1. The effects of these key parameters will be studied with examples of realistic parameter values. The di-

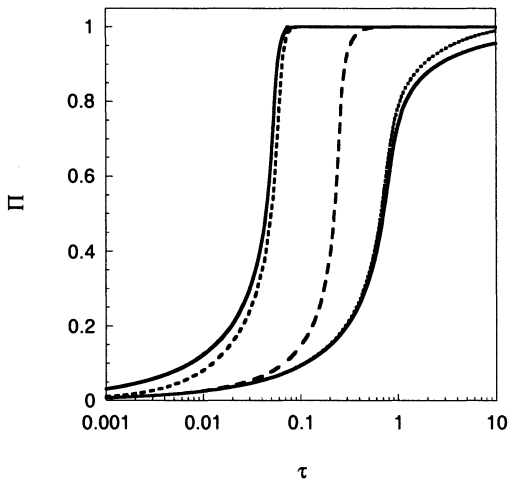

Figure 4. Effect of the dimensionless micellar dissolution rate N_D on the calculated dynamic surface pressure Π at a planar interface with the Langmuir adsorption isotherm when $C_T/C^* = 10$, $K_L C^* = 100$, $N = 64$, $N_l \equiv l/L = 10$, and $N_D = 0, 1, 10^2, 10^4, 10^6$, and 10^8 (overlaps with 10^6), from right to left; here micellar diffusion is not considered, $S \equiv D_N/D_1 = 0$.

mensionless concentrations, $N_C \equiv K_F C^*$, at the cmc for certain nonionic surfactants are between 10 and 600. In the example calculations, we choose $N_C = 100$, which is in the middle of the range just given. The dimensionless diffusion boundary length, N_l, depends on the effective diffusion-layer thickness, l, in the measurements and the characteristic adsorption length, L. It has been shown that for l larger than $10L$ the effect of the diffusion length is negligible in sub-cmc solutions (Liao et al., 2003). Hence, $N_l = 10$, which corresponds to a practically infinite diffusion length, is used for the sample calculations. A smaller value of N_l was found in our experiments (see next section). For spherical micelles, the aggregation number N can range from 50 to 1,000. The values of $N = 64$, 216, or 1,000, which lie in this range and give diffusivity ratios of $D_N/D_1 = N^{-1/3} = 0.25$, 0.16, or 0.1, respectively, are used in the sample calculations.

Figure 4 demonstrates the effects of the dimensionless micellar dissolution rate N_D on the DST at a planar interface. Here the diffusion of micelles is neglected ($D_N/D_1 = 0$) for examining the effects of micellar dissolution separately from the effects of micellar diffusion. For the limit of zero dissolution rate ($N_D = 0$) or with no micelles ($C_T = C^*$), the dimensionless equilibration time for the surface pressure to reach 95% (τ_{95}) of the total pressure increase is more than 10. If micelles are present but dissolve slowly, for example, when $N_D = 1$, τ_{95} decreases little compared to the situation when $N_D = 0$. As N_D increases to 100, τ_{95} drops sharply to 0.5, because of fast micellar dissolution. Moreover, the availability of micelles close to the interface results in release of monomers: the monomers do not need to be transported from longer distances, and thus the penetration depth, d, for monomer concentration is shortened. As N_D increases further, τ_{95} decreases until $N_D \approx 10^4$. Thereafter, further increases in N_D do not result in further increases in the rate at which DST decreases. This phenomenon has not been recognized previously. The existence of such a limit shows that the micelles are converted into monomers quickly and are depleted in a thin layer, which has a length d that is relatively small compared to l. Hence, the adsorption rate is mainly controlled by the diffusion of monomers in this thin layer.

To examine in more detail how micellar dissolution affects the adsorption, Figure 5 compares the concentration profiles for a micellar solution with $C_T = 10$ cmc and $N_D = 10^4$ to those of a sub-cmc solution, $C_T = 0.5$ cmc, at various stages during dynamic adsorption at a planar interface. For the sub-cmc solution, the monomers adsorb first on the air/water surface and deplete the bulk concentration up to $\xi = 0.03$, where $\xi \equiv x/l$, for $\theta = 0.1$. When more molecules are adsorbed, the depleted length becomes longer, for example, $\xi = 0.1$ for $\theta = 0.5$, and $\xi = 0.4$ for $\theta = 0.95$ (Figures 5a–5c). After the adsorption is nearly complete ($\theta > 0.95$), the depleted monomer concentration starts being replenished by diffusion from the bulk until $u_1 = 1$. In this example, d is about 0.5 l. On the contrary, a much smaller value of $d = 0.03$ l is found for the micellar solution (Figures 5d–5f). Thus, for post-cmc solutions, the dissolution of micelles makes the effective depletion length smaller by replenishing the monomers as they are lost to the interface by adsorption. Hence dynamic adsorption from micellar solutions is analogous to dynamic adsorption from premicellar solutions, but with a smaller effective length.

To understand the effects of considering not only micellar dissolution but also micellar diffusion on dynamic adsorption at a planar interface, τ_{95} is plotted at different N_D with various values of N and diffusivity ratios S in Figure 6. In the cases of $N = 64$ with either mobile micelles ($S = 0.25$) or immobile micelles ($S = 0$), τ_{95} decreases with increasing N_D, but reaches different plateaus. The τ_{95} curves for $S = 0$ and $S = 0.25$ overlap when $N_D < 10^3$. With increasing values of N_D, these two curves diverge (3a and 3b in Figure 6) and reach plateaus of 0.06 and 0.02 for $S = 0$ and $S = 0.25$, respectively. We infer that under these conditions, the effect of micellar diffusion is more important in the high dissolution-rate regions, where the micellar concentration gradient is larger because micelles are consumed faster near the interface. For a larger aggregation number $N = 216$, with $S = 0$, τ_{95} can be twice as large as that of $N = 64$ for $N_D = 10^3$. However, for $N_D > 10^5$, τ_{95} is independent of N when $S = 0$. On the contrary, as $S = N^{-1/3}$, when micellar diffusion is considered, the τ_{95} curves are nearly parallel for $N_D > 10$, and τ_{95} is larger with larger N. The difference in the values of τ_{95} for $N = 64$ and 1,000 is about a factor of 4 when $N_D \approx$ 1,000. Thus, for micelle sizes that are not monodisperse, for example, varying from 64 to 1,000, the size effect can alter τ_{95} by up to fourfold depending on the size distribution. Then, a more complex model with a population-balance approach may be needed. On the other hand, if N varies over a smaller range, for example, from 200 to 250, the effect of size distribution on dynamic adsorption may be minor.

The effect of the dimensionless length of the diffusion boundary layer N_l on the DST for adsorption at a planar interface is demonstrated in Figure 7. For a solution with $C_T/C^* = 10$ and a layer thickness $N_l > 10$, the values of τ_{95} for all values of N_D are independent of N_l. When $N_l = 1$, however, τ_{95} values become smaller than the respective val-

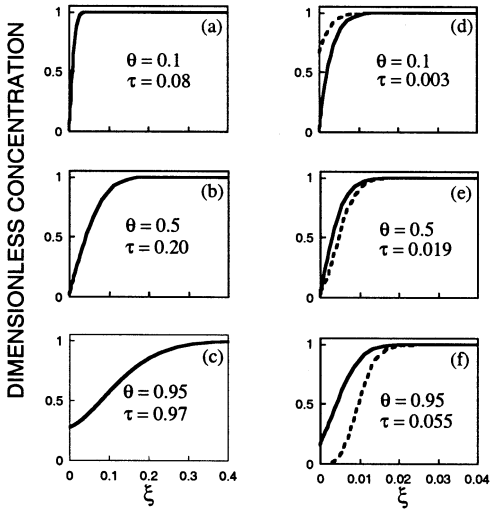

Figure 5. Concentration profiles of submicellar and postmicellar solutions at different stages in the adsorption process with $N_l = 10$, where $\xi \equiv x/l$.

(a)–(c) Concentration profiles for a sub-cmc solution, $T \equiv C_T/C^* = 0.5$ or $N_C = 50$; (d)–(f) monomer (solid lines) and micellar (broken lines) concentration profiles for a micellar solution with $N_C = 100$, $T = 10$, $S = 0$, $N = 64$, and $N_D = 10^4$. Note that the ξ-axis has a larger scale in parts (a)–(c) compared to that in parts (d)–(f).

ues with $N_l = 10$ for $N_D < 10$, where micellar dissolution is not fast enough to replenish the monomer losses, and the monomer concentration has a depletion depth $d > L$. When $N_D > 10$, d becomes smaller than L due to micellar dissolution, and τ_{95} is the same for both $N_l = 1$ and 10. For $N_l = 0.1$ or 0.01, τ_{95} drops with decreasing N_l, but is independent of N_D up to values of N_D of 10^3 or 10^4.

For spherical bubbles, the smaller the value of $N_R \equiv R/l$ is, the larger the adsorption rate is, because the inward radial flux increases with decreasing radius, r. For $N_R > 100$, the equilibration time is found to be essentially the same as that for a planar interface (Figure 8). For $N_R = 1$, $\tau_{95} = 0.85$ for $N_D \le 10$, and then drops to reach another plateau at 0.07 for $N_D \ge 10^4$. For $R < l$, or $N_R < 1$, the effect of curvature is more substantial. For example, for $N_R = 0.1$, τ_{95} starts with a value of 0.09, is independent of N_D up to $N_D = 100$, and then drops to a plateau of 0.03 as N_D increases without bound.

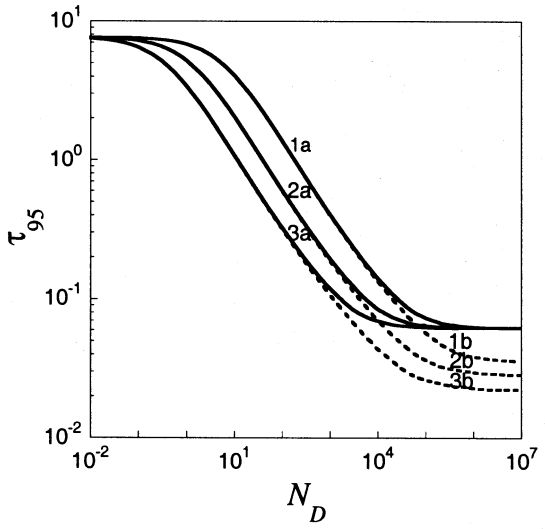

Figure 6. Effect of N_D on τ_{95} for a planar interface with the Langmuir adsorption isotherm when $K_L C^* = 100$, $C_T/C^* = 10$, $l/L = 10$, and various aggregation numbers N.

(1a) $N = 1{,}000$, $S \equiv D_N/D_1 = 0$; (1b) $N = 1{,}000$, $S = 0.1$; (2a) $N = 216$, $S = 0$; (2b) $N = 216$, $S = 0.16$; (3a) $N = 64$, $S = 0$; (3b) $N = 64$, $S = 0.25$.

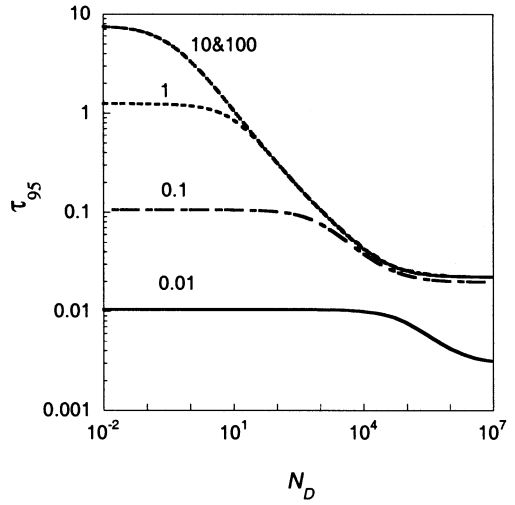

Figure 7. Effect of N_D on equilibration time τ_{95} for $N_C = 100$, $T = 10$, $N = 64$, $S \equiv D_N/D_1 = 0.25$, and various values of N_l as indicated; here the interface is planar ($N_R = \infty$).

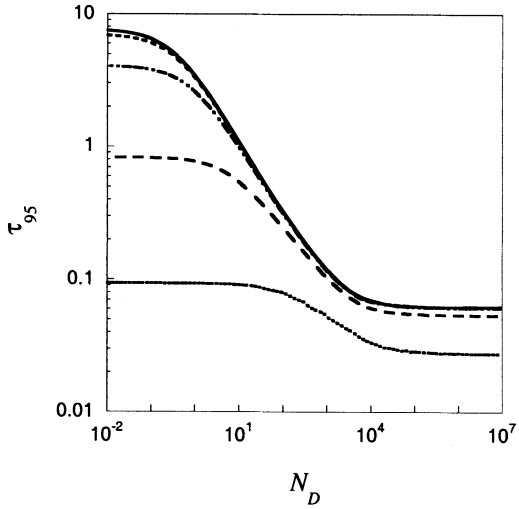

Figure 8. Effects of N_D on equilibration time for $N_C = 100$, $T = 10$, $N = 64$, $S = 0.25$, $N_l = 10$, and dimensionless radius $N_R \equiv R/l = \infty$ (planar interface), 100, 10, 1, and 0.1, from top to bottom.

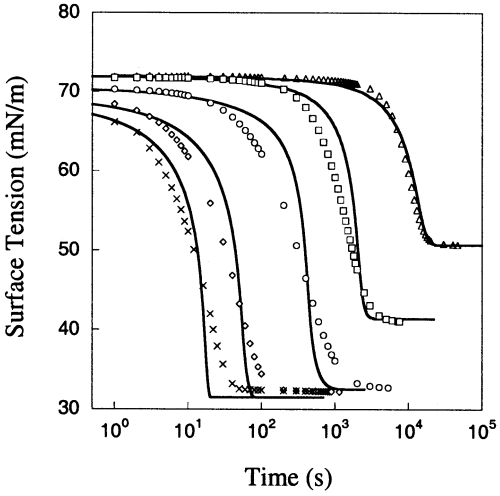

Figure 9. Dynamic surface tension data of aqueous $C_{14}E_6$.

Below the cmc: $T = 0.1$ (0.6 μM; Δ), 0.33 (2 μM; $\square$), and 1.0 (6 μM; $\bigcirc$). Here $\Gamma_{m,L} = 3.7\times10^{-6}$ mol/m^2, $K_L = 1.4\times10^4$ m^3/mol, and $D_1 = 2.84\times10^{-10}$ m^2/s. The value of $l = 0.3$ mm is found to fit the data. Above the cmc: $T = 5$ (30 μM; $\diamond$) and 10 (60 μM; $\times$). Here $N = 216$ and $D_N/D_1 = 0.16$. The value of $1/kC^* = 1.2$ ms with $N_D = 10^6$ is found to fit both sets of data.

Experimental results and fitting to the model

The DST data for $C_{14}E_6$ and $C_{16}E_6$ show the typical behavior of the effect of concentration below and above the cmc (Figures 9 and 10). From the equilibrium data, obtained using solutions of sub-cmc concentrations, we found the best fitted parameters $\Gamma_{m,L}$ and K_L, as detailed in the Material and Methods section (Table 1). From fitting the DST data for the sub-cmc solutions, l was found to be 0.3 mm. For DST equilibrated in less than 10^4 s (0.33 and 1.0 cmc of $C_{14}E_6$), the DST data are lower than the fitted curves at short times, because the effective value of l may be smaller initially due to the convection accompanying surface preparation. Nonetheless, the model with a fixed value of l can capture the basic features of the sub-cmc DST data of the three concentrations examined for both surfactants, indicating that the details of the convective flow can be ignored to a first approximation. Moreover, the diffusion-controlled mechanism applies when l is adjustable as before, showing that the dynamic Langmuir isotherms used are adequate.

Using the same value of $l = 0.3$ mm for the two micellar solutions of $C_{14}E_6$, the best-fitted dissolution time constant $1/kC^*$, or τ_k, was found to be 1.2 ms. The DST data are lower than the fitted curves at short times and higher at longer times. This phenomenon could result from the effective l changing with time, as observed in the sub-cmc DST data. Another possibility is that at high surface density, the adsorption process becomes slower and mixed kinetics should be used. Then, the diffusion-controlled model would predict a faster adsorption rate than observed. Nonetheless, the model can still describe the key features of the micellar solution data, namely, that the DST curves shift to smaller times as C_T increases. Similar results were obtained for $C_{16}E_6$ (Figure 10). Using $l = 0.3$ mm, $N = 216$, and $S = 0.16$, τ_k was found to be 4.5 ms. The time constant of $C_{16}E_6$ is larger than of $C_{14}E_6$ because $C_{16}E_6$ is more hydrophobic, having a lower cmc, and apparently lower dissolution rate.

The calculated spatial profiles of the monomer and micellar concentrations for 60 μM $C_{14}E_6$ with the same fitted parameters as in Figure 9 are shown in Figure 11. During the adsorption process, the micelles near the interface dissociate and create a depleted micellar zone with a length d, where the micellar concentration decreases sharply toward the interface and the monomer concentration is kept at cmc. It is noticeable that the monomer concentration profile is about a straight line within $x = d$, and the adsorption rate, or the slope, is ca. C^*/d. The value of d is about the same for both cases, with or without diffusion, when $\theta < 0.1$ For $\theta > 0.1$, d increases faster in the case of $S = 0$ because micelles cannot be supplied via bulk diffusion. Hence, the adsorption rate is smaller for $S = 0$ and the resulting τ_{50} and τ_{95} are larger (by a factor of 2) than that for $S = 0.16$. The maximum values of d are about 24 μm for $S = 0.16$ and 60 μm for $S = 0$. Fluorescence data reported recently by Song et al. (2002) for aqueous $C_{14}E_6$ micellar solutions show supporting evidence that there is a micellar depletion region with thickness between 10 to 100 μm.

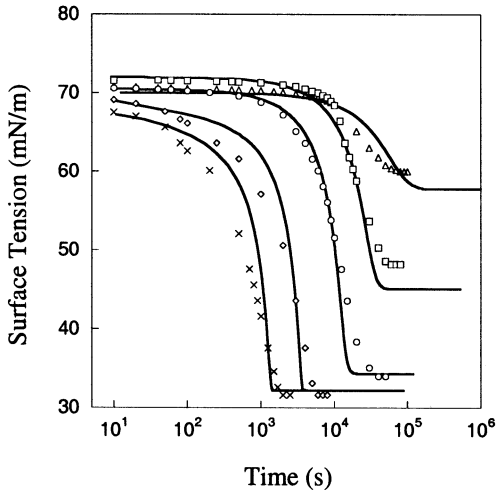

Figure 10. Dynamic surface tension data of aqueous $C_{16}E_6$.

Below the cmc: $T = 0.2$ (0.1 μM; $\triangle$), 0.5 (0.25 μM; $\square$), and 0.9 (0.45 μM; $\bigcirc$). Here $\Gamma_{m,L} = 6\times10^{-6}$ mol/m^2, $K_L = 2.65\times10^4$ m^3/mol, and $D_1 = 2.79\times10^{-10}$ m^2/s. The value of $l = 0.3$ mm is found to fit the data. Above the cmc, $T = 10$ (5 μM; $\diamond$) and 20 (10 μM; $\times$). Here $N = 216$ and $D_N/D_1 = 0.16$. The value of $1/kC^* = 4.5$ ms with $N_D = 10^8$ is found to fit both sets of data.

Conclusions

A one-dimensional model is developed for the diffusion-controlled dynamic adsorption and surface tension in micellar solutions of nonionic surfactants. The micelles are assumed to be monodisperse, of fixed aggregation number, N, and with a diffusivity estimated from the Stokes-Einstein equation. The micellar dissolution rate is described as being proportional to the micellar concentration and to the concen-

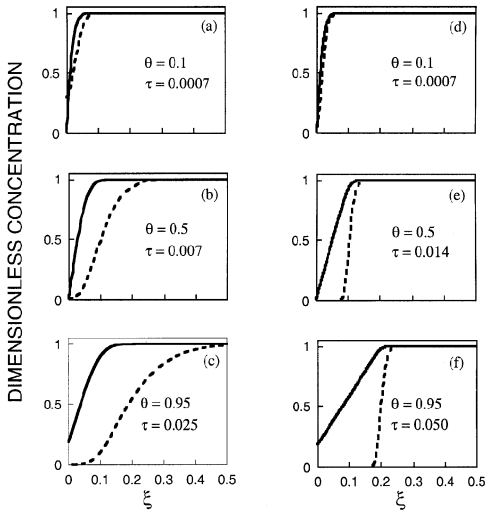

Figure 11. Calculated monomer (solid lines) and micellar (broken lines) concentration profiles for $C_{14}E_6$ micellar solutions at different stages in the adsorption process.

Parameters used are $N_C = 84$, $l = 0.3$ mm or $N_l = 0.5$, $T = 10$, $N = 216$, and $N_D = 10^6$: (a)–(c) with micellar diffusion, $S = 0.16$; (d)–(f) without micellar diffusion, $S = 0$. Accounting for micellar diffusion, the micelle depletion region decreases from 0.2 l ($x = 60$ μm) to 0.08 l ($x = 24$ μm).

tration difference between the cmc and the local monomer concentration. The micellar dissolution is incorporated into a diffusion-controlled adsorption model with the Langmuir or Frumkin adsorption isotherm. The hydrodynamic effects due to interface generation in the experiments are simplified as resulting in an effective stagnant layer with a finite length, l, which is an adjustable parameter that can be obtained from the sub-cmc DST data. The model is solved rigorously by a finite-element algorithm, without any linearization further approximations. A stretched grid and adaptive time stepping are used to optimize computational efficiency without losing accuracy.

This model covers mostly the dissolution of micelles. The stepwise kinetics of micellization, as detailed by Aniansson and Wall (1974), is simplified to a monodisperse micellar model. The dissolution rate constant, k, is related to the reciprocal of the fast micellar relaxation time, τ_1, as indicated by Fainerman (1981). Further improvement of this model can include the use of the mixed kinetics model, which may be needed when dissolution/diffusion become faster. For pulsating area conditions, where desorption may occur and micelles are formed from monomers, a more complex model than Eq. 3 is needed. Such a model is beyond the scope of this article, and is the subject of future investigation.

Simulations were done to test the relative importance of several key dimensionless parameters on the adsorption rate. The dimensionless equilibration time, τ_{95}, is found to depend strongly on the dimensionless dissolution rate, $N_D \equiv \tau_D k C^*$. Larger values of N_D result in smaller values of τ_{95}. The calculated concentration profiles show that the micellar dissolution decreases the penetration depth, d, and hence adsorption in micellar solutions is analogous to premicellar adsorption with a shorter l. The value of τ_{95} also depends on the dimensionless diffusion length, $N_l = l/L$, and the dimensionless bubble radius, $N_R \equiv R/l$. The diffusion of micelles is also considered. The diffusivity of micelles D_N is estimated from the Stokes-Einstein equation, and the ratio of D_N to the monomer diffusivity, D_1, is given by $S \equiv D_N/D_1 = N^{-1/3}$, where N is the aggregation number. When $N_D > 10^4$, where the micellar concentration gradient is large, the diffusion of micelles is found to be important. When micellar sizes range from 64 to 1,000, τ_{95} can vary up to fourfold. On the contrary, when the size distribution is narrow, the effects of variable N are minor; then, the assumption of monodisperse micelles is well justified.

New equilibrium and dynamic surface-tension data for a planar interface were obtained for two nonionic surfactants, $C_{14}E_6$ and $C_{16}E_6$, at 24°C at concentrations of 0.6–60 μM ($T \equiv C_T/C^* = 0.1$ to 10) and 0.1–10 μM ($T = 0.2$ to 20), respectively. The equilibration times for $C_{14}E_6$ decrease from 10^3–10^4 s below the cmc to 30–100 s above the cmc. For $C_{16}E_6$ the times decrease from 10^4–10^5 s below the cmc to 10^3–6×10^3 s above the cmc. The data were used to obtain the Langmuir isotherm parameters $\Gamma_{m,L}$ and K_L, the effective diffusion length l (≈ 0.3 mm), and the micellar dissolution time constant $\tau_k \equiv 1/kC^*$. The model fitted the data fairly well, despite the simplified assumptions used. The same values of τ_k, 1.2 ms for $C_{14}E_6$ and 4.5 ms for $C_{16}E_6$, fitted data at two micellar concentrations. The latter surfactant has a lower cmc and a smaller dissolution rate, probably because it is more hydrophobic. The values of τ_k can be used to predict DSTs for micellar solutions of higher concentrations, for which data may not be available if the equilibration times are too low.

Acknowledgments

This research was supported in part by grants from the National Science Foundation (Grant CTS 0135317) and the National Institutes of Health (Grant HL 54641-02) to Elias I. Franses, and grants from the Basic Energy Sciences Program of the U.S. Department of Energy (Grant DE-FG02-96ER14641) and the Purdue Research Foundation to Osman A. Basaran.

Literature Cited

Aniansson, E. A. G., and S. N. Wall, "On the Kinetics of Step-Wise Micelle Association," *J. Phys. Chem.*, **78**, 1024 (1974).

Chang, C.-H., and E. I. Franses, "Modified Langmuir-Hinshelwood Kinetics for Dynamic Adsorption of Surfactants at the Air/Water Interface," *Colloids Surf.*, **69**, 189 (1992).

Chang, C.-H., and E. I. Franses, "Adsorption Dynamics of Surfactants at the Air/Water Interface: A Critical Review of Mathematical Models, Data, and Mechanisms," *Colloids Surf. A*, **100**, 1 (1995).

Cussler, E. L., *Diffusion*, Cambridge Univ. Press, London (1984).

Dukhin, S. S., G. Kretzschmar, and R. Miller, *Dynamics of Adsorption at Liquid Interfaces*, Elsevier, Amsterdam (1995).

Dushkin, C. D., "Model of the Quasi-Monodispersed Micelles with Application to the Kinetics of Micellization, Adsorption and Diffusion in Surfactant Solutions and Thin Films," *Colloids Surf. A*, **143**, 283 (1998).

Dushkin, C. D., I. B. Ivanov, and P. A. Kralchevsky, "The Kinetics of Surface Tension of Micellar Surfactant Solutions," *Colloids Surf.*, **60**, 235 (1991).

Evans, D. F., and H. Wennerström, *The Colloidal Domain*, 2nd ed., Chap. 4, Wiley, New York (1999).

Fainerman, V. B., "Kinetics of Surfactant Adsorption from Micellar Solutions," *Kolloidn Zh.*, **43**, 94 (1981).

Fainerman, V. B., Y. M. Rakita, and V. M. Zadara, "Diffusion-Controlled Kinetics of the Adsorption from Solutions of Surface-Active Substance Containing Micelles," *Zh. Fiz. Khim.*, **58**, 2006 (1984).
Ferri, J. K., and K. J. Stebe, "Which Surfactants Reduce Surface Tension Faster? A Scaling Argument for Diffusion-Controlled Adsorption," *Adv. Colloid Interface Sci.*, **85**, 61 (2000).
Filippov, L. K., and N. L. Filippova, "Dynamic Surface Tension and Adsorption Kinetics from Micellar Solutions on Planar Surfaces," *J. Colloid Interface Sci.*, **187**, 304 (1997).
Franses, E. I., O. A. Basaran, and C.-H. Chang, "Techniques to Measure Dynamic Surface Tension," *Curr. Opin. Colloid Interface Sci.*, **1**, 296 (1996).
Hill, C. G., *An Introduction to Chemical Engineering Kinetics and Reactor Design*, Wiley, New York (1977).
Knupp, P., and S. Steinberg, *The Fundamentals of Grid Generation*, CRC Press, Boca Raton, FL (1993).
Liao, Y.-C., E. I. Franses, and O. A. Basaran, "Computation of Dynamic Adsorption with Adaptive Integral, Finite Difference, and Finite Element Methods," *J. Colloid Interface Sci.*, **258**, 310 (2003).
Lin, S.-Y., K. McKeigue, and C. Maldarelli, "Diffusion-Controlled Surfactant Adsorption Studied by Pendant Drop Digitization," *AIChE J.*, **36**, 1785 (1990).
Lucassen, J., "Adsorption Kinetics in Micellar Systems," *Faraday Discuss. Chem. Soc.*, **72**, 76 (1976).
Luskin, M., and R. Rannacher, "On the Smoothing Properties of Crank-Nicholson Scheme," *Appl. Anal.*, **14**, 117 (1982).
Miller, R., "Adsorption Kinetics of Surfactants from Micellar Solutions," *Colloid Polym. Sci.*, **259**, 1124 (1981).
Nagarajan, R., and E. Rukenstein, *Equations of State for Fluids and Fluid Mixtures*, Chap. 15, Elsevier, Amsterdam (2000).
Noskov, B. A., "Kinetics of Adsorption from Micellar Solutions," *Adv. Colloid Interface Sci.*, **95**, 237 (2002).
Patist, A., S. G. Oh, R. Leung, and D. O. Shah, "Kinetics of Micellization: Its Significance to Technological Processes," *Colloids Surf. A*, **176**, 3 (2001).
Pillai, V., and D. O. Shah, eds., *Dynamic Properties of Interfaces and Association Structures*, Chap. 5, AOCS Press, Champaign, IL (1995).
Rosen, M. J., *Surfactants and Interfacial Phenomena*, Wiley, New York (1978).
Schunk, P. R., *Surfactant and Polymer Additives in Coating and Related Flows*, PhD Thesis, Univ. of Minnesota, Minneapolis (1989).
Song, Q., and C. Maldarelli, "Surfactant Transport to an Initial Clean Fluid Interface from Micellar Solution: Theoretical and Experimental Study," AIChE Meeting, Indianapolis, IN (2002).
Strang, G., and G. J. Fix, *An Analysis of the Finite Element Method*, Prentice Hall, Englewood Cliffs, NJ (1973).
Ward, A. F. H., and L. Tordai, "Time-Dependence of Boundary Tensions of Solutions," *J. Chem. Phys.*, **14**, 453 (1946).
Zhang, X., R. S. Padgett, and O. A. Basaran, "Nonlinear Deformation and Breakup of Stretching Liquid Bridges," *J. Fluid Mech.*, **329**, 297 (1996).
Zhmud, B. V., F. Tiberg, and J. Kizling, "Dynamic Surface Tension in Concentrated Solutions of CnEm Surfactants: A Comparison Between the Theory and Experiment," *Langmuir*, **16**, 2557 (2000).

Manuscript received Jan. 15, 2003, and revision received May 9, 2003.